MIXING OF STRUCTURES IN ^{100}Zr STUDIED VIA β DECAY*

D. Kalaydjieva [a,b], V. Bildstein[a], P.E. Garrett[a], M. Zielińska[b]
K. Stoychev[a], M. Rocchini[a,c], S. Pannu[a], H. Bidaman[a]
W. Korten[b], V. Vedia[d], A.B. Garnsworthy[d], Z. Ahmed[a]
C. Andreoiu[e], D.W. Annen[e], H. Asch[e], A.A. Avaa[d], G.C. Ball[d]
G. Benzoni[f], S.S. Bhattacharjee[d], S. Buck[a], R.J. Coleman[a]
S. Devinyak[d], I. Dillmann[d], J. Dowie[g], R. Caballero-Folch[d]
F.H. Garcia[h], E.D. Geerlof[d], B. Greaves[a], C.J. Griffin[d]
A.L. Grimes[d], G.F. Grinyer[i], E. Gyabeng Fuakye[i], G. Hackman[d]
S. Hicks[g], D. Hymers[a], R. Kanungo[j], K. Kapoor[i]
V. Karayonchev[k], E. Kasanda[a], S. Lange[a], B. Lenardo[l]
L. Maqungo[m], N. Marchini[c], B. Marlow[d], M.S. Martin[e]
K.M. Mashtakov[a], S. Murillo Morales[d], J.R. Murias[d]
A. Nannini[c], C. Natzke[d], B. Olaizola[n], K. Ortner[e], E. Peters[g]
C.M. Petrache[e,o], M. Polletini[f], C. Porzio[h], A.J. Radich[a]
G. Richardson[l,p], N. Saei[i], M. Satrazani[q], M. Scheck[r]
M. Siciliano[k], M. Singh[j], P. Spagnoletti[e], C.E. Svensson[a,d]
E. Taddei[e], G. Tocabens[b], D.A. Torres[d,s], S. Triambak[m]
R. Umashankar[d], S. Valbuena[a], F. Wu[e], T. Zidar[a]

[a]University of Guelph, Guelph, N1G 2W1, ON, Canada
[b]IRFU, CEA, Université Paris-Saclay, Gif-sur-Yvette, 91191, France
[c]INFN Sezione di Firenze, Firenze, 50019, Italy
[d]TRIUMF, Vancouver, V6T 2A3, BC, Canada
[e]Simon Fraser University, Burnaby, V5A 1S6, BC, Canada
[f]INFN Sezione di Milano, Milano, 20133, Italy
[g]University of Kentucky, Lexington, 40506, KY, USA
[h]Lawrence Berkeley National Laboratory, Berkeley, 94720, CA, USA
[i]University of Regina, Regina, S4S 0A2, SK, Canada
[j]Saint Mary's University, Halifax, B3H 3C3, NS, Canada
[k]Argonne National Laboratory, Lemont, 60439, IL, USA
[l]SLAC National Accelerator Laboratory, Menlo Park, 94025, CA, USA
[m]University of the Western Cape, Bellville, 7535, South Africa
[n]CERN, Geneva, 1211, Switzerland
[o]CNRS/IN2P3, IJCLab, Université Paris-Saclay, Orsay, 91405, France
[p]Yale University, New Haven, 06511, CT, USA
[q]University of Liverpool, Liverpool, L69 7ZE, United Kingdom
[r]Scottish Universities Physics Alliance, Glasgow, G12 8QQ, United Kingdom
[s]Universidad Nacional de Colombia, Bogotá, 111321, Colombia

Received 16 November 2025, accepted 31 January 2026, published online 31 March 2026

* Presented at the XXXVIII Mazurian Lakes Conference on Physics, Piaski, Poland, August 31–September 6, 2025.

Properties of low-lying states in ^{100}Zr were studied using the GRIFFIN spectrometer at TRIUMF following the β decay of ^{100}Y. Using γ–γ angular correlations, level spins were confirmed and E2/M1 mixing ratios determined with improved precision. Applicability of a two-state mixing model to the observed structures in ^{100}Zr is explored.

DOI:10.5506/APhysPolBSupp.19.1-A15

1. Low-energy structures in ^{100}Zr

The Zr isotopes are known to undergo a sudden ground-state shape transition at $N = 60$. This is reflected by rapid changes of their charge radii [1], excitation energies of the 2^+_1 states, and $B(\mathrm{E2}; 2^+_1 \to 0^+_1)$ values [2]. The reproduction of the energy and $B(\mathrm{E2})$ systematics for the Zr isotopes spanning the transition at $N = 60$ has recently been achieved thanks to advances with the Monte-Carlo Shell Model (MCSM) [3]. At the same time, the MCSM calculations suggested the appearance of multiple shape coexistence in ^{100}Zr, with a spherical state at about 1.5 MeV that coexists with the well-deformed prolate ground state and excited 0^+_2 and 0^+_3 states that are oblate and prolate, respectively.

A different level structure is proposed by calculations employing the interacting boson model with configuration mixing (IBM-CM) [4], which suggest that a spherical normal configuration, associated with the 0^+_2 state, coexists with a weakly-deformed intruder configuration.

Based on the similarity of the decay of the 0^+_2 state in ^{100}Zr with the corresponding state in the $N = 60$ isotone ^{98}Sr [5], a spherical, or very weakly-deformed oblate shape can be inferred [2, 6]. This appears to be in better agreement with the IBM-CM picture. While both models describe remarkably well the collectivity in the ground-state band of ^{100}Zr, the experimental $B(\mathrm{E2}; 0^+_2 \to 2^+_1)$ value is successfully reproduced only by the IBM-CM calculations [4]. On the other hand, evidence for a band structure built on the 0^+_2 state, involving the 2^+_2 state, was reported [6].

The 2^+_3 state at 1196 keV was a candidate to be the bandhead of a γ band proposed in Ref. [7]. However, observation of a transition from this state to the 0^+_3 level [8] raised the possibility of its assignment as the spin-2 member of a rotational band built on the 0^+_3 state. In the present work, we focus on investigating the properties of the 2^+_2 and 2^+_3 states.

2. Measurement of ^{100}Y β decay at TRIUMF-ISAC

Low-spin excited states in ^{100}Zr were populated in the β decay of the $(1)^-$ state of ^{100}Y ($T_{1/2} = 732$ ms [9]), following β decay of ^{100}Sr. Radioactive $A = 100$ ions were produced by bombarding a UC_x target with a 9.8 μA

proton beam, delivered by the TRIUMF 500 MeV cyclotron, followed by ionization and mass separation of reaction products. The resulting beam mixture of ^{100}Rb (5×10^4/s) and ^{100}Sr (2×10^4/s) was transported to the Isotope Separator and ACcelerator (ISAC I) facility, and delivered onto a Mylar tape at the center of the GRIFFIN spectrometer [10]. The 15 HPGe clover detectors of GRIFFIN were arranged in "optimized peak-to-total" configuration [10] and BGO shields were used to reject Compton-scattering events. The data were collected in a triggerless mode with a repeating acquisition cycle (3.5 s of beam deposition followed by 1 s of measurement of the decay, after which the tape was moved and the cycle repeated). They were sorted using the "addback" procedure, and a cross-talk correction was introduced to account for the signal distortion due to events occurring in the adjoining crystals [10, 11].

3. γ–γ angular correlations

The spin of an excited nuclear state can be deduced from the angular distribution of γ rays emitted in its decay if its magnetic substates are not equally populated. In β decay, the γ-ray angular distributions are isotropic, however, if the γ rays are emitted in a cascade, the direction of one of them can be used to define an orientation axis and effectively generate an alignment. The angular correlations between subsequent γ rays have distinct patterns as a function of the relative angle, which depend on the spins of the involved states and the multipolarities of the emitted γ rays. For γ-ray cascades involving dipole or quadrupole transitions, the angular correlations $W(\theta)$ can be described by

$$W(\theta) = A_{00}\left[1 + a_2Q_2P_2(\cos\theta) + a_4Q_4P_4(\cos\theta)\right] ,$$

where A_{00} is the γ–γ coincidence intensity, $P_L(\cos\theta)$ are Legendre polynomials of order L, a_i are coefficients that depend on the involved spins and multipolarities, and Q_L are attenuation factors related to the finite detector size. To account for the latter, a detailed Geant4 Monte-Carlo simulation of GRIFFIN was developed (see Ref. [12] and references therein). Considering that $W(\theta)$ is a linear combination of Legendre polynomials scaled with the angular correlation coefficients a_2 and a_4, any correlation can be described by a combination of basis correlations $Z_i(\theta)$ with probability distributions given by the Legendre polynomials

$$W(\theta) = A_{00}\left[(1 - a_2 - a_4)Z_0(\theta) + a_2Z_2(\theta) + a_4Z_4(\theta)\right] ,$$

where $Z_0(\theta) = 1$, $Z_2(\theta) = 1 + Q_2P_2(\cos\theta)$, and $Z_4(\theta) = 1 + Q_4P_4(\cos\theta)$. By fitting an experimental correlation with the simulated $Z_i(\theta)$ basis functions, the corresponding a_2 and a_4 parameters can be extracted.

In addition to the solid-angle attenuation, the observed angular correlations may deviate from their expected theoretical form due to differences in the detector efficiencies and data-acquisition dead-time effects. To account for those, the so-called "mixed-events" technique can be applied [12] in which an isotropic angular distribution is constructed from time-uncorrelated events from the same data set and used for normalization.

4. Results

The data were sorted into γ–γ matrices using a $\pm$300 ns prompt-coincidence time window for each opening angle θ_i. The γ-ray hits with absolute time differences from 500 to 1800 ns were considered to be time-uncorrelated and were organized into time-random coincidence matrices, which were scaled and subtracted from the prompt matrices. In addition, the mixed-events matrices were produced for each opening angle, using time-uncorrelated γ–γ events, involving HPGe hits separated by more than 2 μs.

In the present study, cascades of the $I \rightarrow 2_1^+ \rightarrow 0_1^+$ type were investigated. For each opening angle θ_i, a coincidence gate was placed on the $2_1^+ \rightarrow 0_1^+$ transition in order to extract the number of counts N_i^{P} in the $I \rightarrow 2_1^+$ transition in the projected spectrum, or *vice versa*. The mixed-events matrices were treated using the same gating and fitting conditions to extract the numbers of counts N_i^{M} corresponding to an isotropic angular distribution. The final angular correlations were given by the ratio $N_i^{\mathrm{P}}/N_i^{\mathrm{M}}$, scaled with a global normalization coefficient $\sum_i N_i^{\mathrm{M}} / \sum_i N_i^{\mathrm{P}}$.

4.1. Examples of angular correlations with GRIFFIN

The angular correlations obtained for the $0_3^+ \rightarrow 2_1^+ \rightarrow 0_1^+$ cascade are presented in the left panel of Fig. 1. The dashed red line denotes the theoretically-expected correlation, which does not follow the experimental data due to the attenuation effects. To account for those, the $Z_{0,2,4}$ basis correlations were simulated with Geant4 and used to construct a large set of template angular correlations corresponding to various combinations of spins and mixing ratios δ. The templates were then compared to the experimental data at each opening angle, and a χ^2/NDF distribution as a function of the mixing ratio was calculated for each assumed spin. The result of this procedure is presented in the right panel of Fig. 1.

Following the recommendation of Ref. [13], the solutions with a χ^2/NDF value small enough to belong to the region encompassing 99% of the total probability distribution are considered as possible assignments. The combinations of spins and mixing ratios which result in a χ^2/NDF value above this limit can be rejected at 99% confidence level. Thus, the only possible spin assignment for the state in question is 0, in agreement with previous stud-

ies [8, 14]. In addition, the solid blue curve in the left panel of Fig. 1 represents the simulated correlations corresponding to the best $\chi^2_{\rm min}/{\rm NDF} = 1.19$ solution in the right panel of Fig. 1. The curve connects the values resulting from the simulation performed for each θ_i with a shaded area illustrating the corresponding statistical uncertainty.

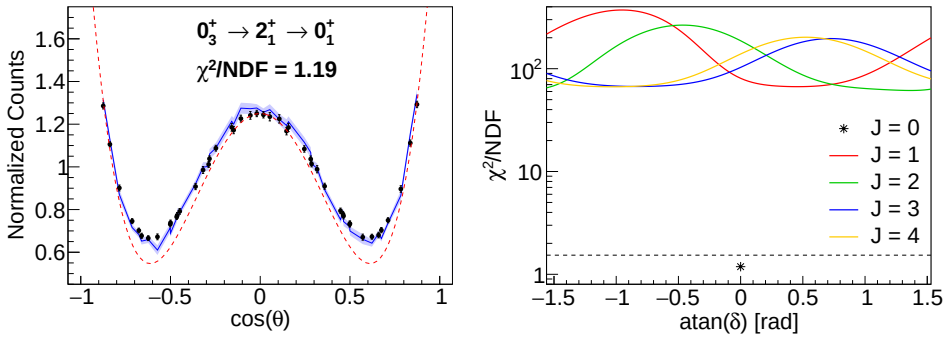

Fig. 1. (Colour on-line) Left panel: Angular correlation for the $0^+_3 \rightarrow 2^+_1 \rightarrow 0^+_1$ cascade. The dashed red line corresponds to the theoretical angular correlation without corrections for finite detector size effects expected for a $0^+ \rightarrow 2^+ \rightarrow 0^+$ cascade with $a_2 = 0.357$ and $a_4 = 1.143$. The solid blue curve represents the Geant4 simulation corresponding to the parameters yielding the best χ^2/NDF value. Right panel: Reduced χ^2 values for different combinations of the adopted spin of the initial state and mixing ratio δ. The solutions corresponding to χ^2 values above the black dashed line can be excluded at a 99% confidence level.

The preliminary results obtained for the $2^+_2 \rightarrow 2^+_1 \rightarrow 0^+_1$ cascade are summarized in Fig. 2, with the best fit ($\chi^2_{\rm min}/{\rm NDF} = 1.02$) corresponding to spin 2 and a mixing ratio of $4.7^{+1.5}_{-1.1}$. Other spin assignments can be rejected at a 99% confidence level. The uncertainty of δ is obtained from the limits of the $\chi^2_{\rm min}+1$ region [13]. The $2^+_2 \rightarrow 2^+_1$ transition was previously measured to have a mixing ratio of $\delta = 8^{+36}_{-4}$ [8], and our angular-correlation data confirm its nearly pure E2 character [11] with increased precision.

The preliminary correlations for the $2^+_3 \rightarrow 2^+_1 \rightarrow 0^+_1$ cascade are presented in Fig. 3. The best fit of the experimental data ($\chi^2_{\rm min}/{\rm NDF} = 1.38$) is achieved for spin 2 and a mixing ratio $\delta = -1.00^{+0.18}_{-0.14}$. The present result is in agreement with the literature value of $-1.0^{+0.8}_{-0.4}$ [8], but has a significantly improved precision.

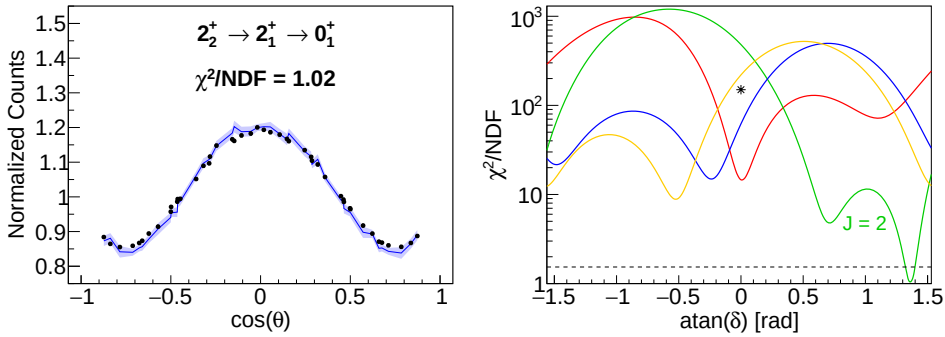

Fig. 2. (Colour on-line) The same as Fig. 1 but for the $2_2^+ \to 2_1^+ \to 0_1^+$ cascade.

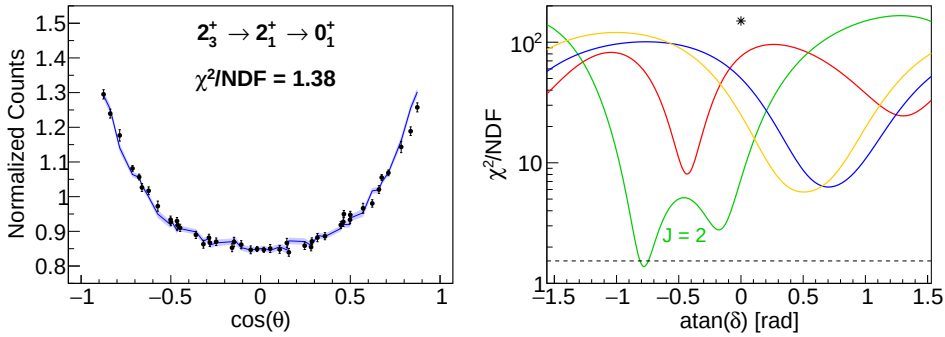

Fig. 3. (Colour on-line) The same as Fig. 1 but for the $2_3^+ \to 2_1^+ \to 0_1^+$ cascade.

4.2. Mixing of structures in ^{100}Zr

Figure 4 shows a partial level scheme of ^{100}Zr, including the 0_1^+, 0_2^+, and 0_3^+ states and their suggested 2^+ band members. Only the $2_i^+ \to 2_f^+$ and $2_i^+ \to 0_f^+$ transitions are shown, with their relative B(E2) values normalized to 1 for the in-band transitions. Pure E2 multipolarity is adopted for the $2_3^+ \to 2_2^+$ transition. The calculated out-of-band $B(\mathrm{E2}, 2_2^+ \to 2_1^+)$ value is 1.24(13) times greater than the in-band transition strength. This can be contrasted with the result for the 2_3^+ level with a $B(\mathrm{E2}; 2_3^+ \to 2_1^+)$ of only $3.6^{+2.4}_{-1.5}$% of the $B(\mathrm{E2}; 2_3^+ \to 0_3^+)$ value. We explore the mixing of the configurations below.

We first consider the mixing of the 0_1^+ and 0_2^+ states. A β_2 deformation of ≈ 0.35 is adopted for the ground state from $B(\mathrm{E2}; 2_1^+ \to 0_1^+) = 77(2)$ W.u. [9]. Using $\rho^2(\mathrm{E0}; 0_2^+ \to 0_1^+) = 0.102(5)$ [15] and the relation between ρ^2(E0) and the mixing amplitude a

$$\rho^2\left(\mathrm{E0}; 0_2^+ \to 0_1^+\right) = \left(\frac{3Z}{4\pi}\right)^2 a^2\left(1-a^2\right)\left[\Delta\left(\beta_2^2\right)\right]^2, \qquad (1)$$

with the assumption of $\beta_2 \ll 0.35$ for the excited 0^+ configuration, leads to the conclusion that the 0^+ states are 92% pure. To simplify our exploration of the two-state mixing model for the $2^+_{1,2}$ states, we consider the 0^+ states as being 100% pure.

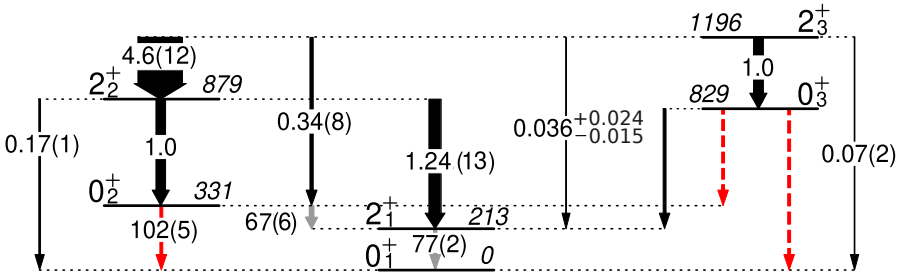

Fig. 4. (Colour on-line) Partial level scheme of ^{100}Zr showing the states suggested to belong to the 0^+_1, 0^+_2, and 0^+_3 bands. The transitions in black are labelled with their relative B(E2) values, calculated using the newly obtained mixing ratios and branching ratios from Ref. [8]. Those in light gray are denoted with their absolute B(E2) values in W.u. [9], whereas E0 transitions are represented by red/dark gray arrows with their $10^3 \times \rho^2$(E0) values [15]. Dashed arrows are unobserved transitions.

We assume that the physical 2^+_1 and 2^+_2 states are linear combinations of 2^+_A and 2^+_B unperturbed configurations

$$|2^+_1\rangle = \alpha|2^+_A\rangle + \beta|2^+_B\rangle\,, \qquad |2^+_2\rangle = -\beta|2^+_A\rangle + \alpha|2^+_B\rangle \tag{2}$$

and that the E2 matrix elements connecting configurations A and B are equal to zero. The lack of a full set of E2 matrix elements precludes the approach presented in *e.g.* Ref. [16], requiring that we make additional assumptions. Assuming an axial shape and $\beta_2 = 0.35$ extracted above, the quadrupole moment $|Q_s(2^+_1)|$ is ≈ 1.05 eb leading to the diagonal matrix element $\langle 2^+_1\|\mathrm{E2}\|2^+_1\rangle \approx 1.4$ eb. Using $B(\mathrm{E2}, 0^+_2 \to 2^+_1)$ of 67(6) W.u. [9] and

$$\langle 0^+_1\|\mathrm{E2}\|2^+_1\rangle = \alpha\langle 0^+_A\|\mathrm{E2}\|2^+_A\rangle\,, \qquad \langle 0^+_2\|\mathrm{E2}\|2^+_2\rangle = \alpha\langle 0^+_B\|\mathrm{E2}\|2^+_B\rangle\,, \tag{3}$$

$$\langle 0^+_1\|\mathrm{E2}\|2^+_2\rangle = -\beta\langle 0^+_A\|\mathrm{E2}\|2^+_A\rangle\,, \qquad \langle 0^+_2\|\mathrm{E2}\|2^+_1\rangle = \beta\langle 0^+_B\|\mathrm{E2}\|2^+_B\rangle\,, \tag{4}$$

we obtain $\alpha^2 = 0.85$ from the B(E2) ratio for the decay of the 2^+_2 state to the 0^+ states. We then use these results together with

$$\langle 2^+_1\|\mathrm{E2}\|2^+_1\rangle = \alpha^2\langle 2^+_A\|\mathrm{E2}\|2^+_A\rangle + \beta^2\langle 2^+_B\|\mathrm{E2}\|2^+_B\rangle\,, \tag{5}$$

$$\frac{B(\mathrm{E2}; 2^+_2 \to 2^+_1)}{B(\mathrm{E2}; 2^+_2 \to 0^+_2)} = \frac{\alpha^2\beta^2\left|\langle 2^+_A\|\mathrm{E2}\|2^+_A\rangle - \langle 2^+_B\|\mathrm{E2}\|2^+_B\rangle\right|^2}{\alpha^2|\langle 0^+_B\|\mathrm{E2}\|2^+_B\rangle|^2}\,, \tag{6}$$

which, under the assumed zero quadrupole moment for the B configuration, results in a maximum predicted ratio in Eq. (6) of 0.33, rather than the observed 1.24. Thus, it is not possible to explain the observed decay pattern with the assumptions used here and a two-state mixing model.

The weak relative E2 transitions from the 2_3^+ state to the ground-state band are indicative of weak mixing of these configurations. No E0 transitions from the 0_3^+ state to the lower 0^+ states have been reported, nor limits set. Figure 5 displays the γ-ray spectrum observed in coincidence with the sum of gates on γ rays feeding the 0_3^+ level. A significant E0-decay branch to the 0_2^+ level would result in the observation of the 118-keV $0_2^+ \rightarrow 2_1^+$ transition. As indicated in Fig. 5, no peak at this energy is present. We set a preliminary upper limit at the 95% confidence level on the $0_3^+ \rightarrow 0_2^+$ branch to be 0.2% of the 616-keV $0_3^+ \rightarrow 2_1^+$ transition intensity, from which we determine $X(\mathrm{E0/E2}) < 0.4$. Unfortunately, no conclusions can be reached as this limit is not overly restrictive; for $B(\mathrm{E2}; 0_3^+ \rightarrow 2_1^+) = 10$ W.u., $\rho^2(\mathrm{E0}; 0_3^+ \rightarrow 0_2^+) < 0.12$.

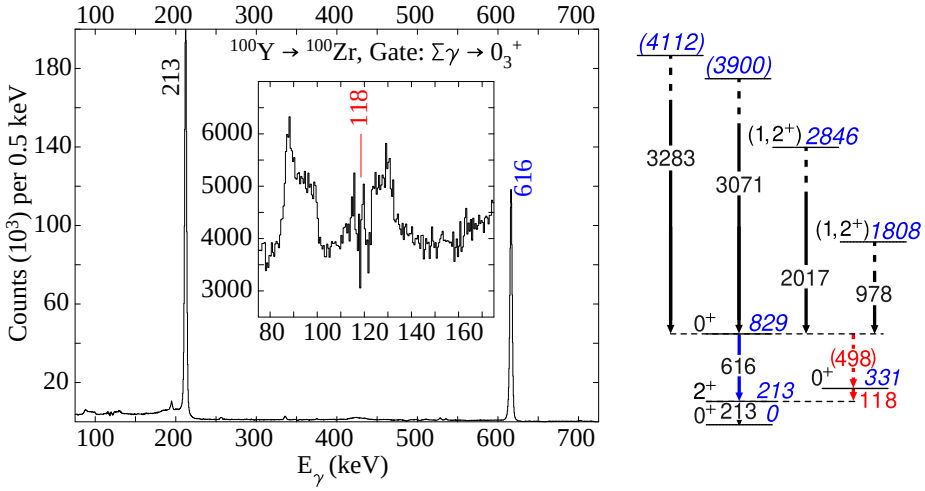

Fig. 5. Portion of the summed γ-ray spectrum (left) observed in coincidence with the 978, 2017, 3071, and 3283 keV γ rays feeding the 0_3^+ level. The latter two originate from newly found states at 3900 keV and 4112 keV. A significant E0 branch to the 0_2^+ state would result in the presence of the 118 keV γ ray in the spectrum; its non-observation leads to an upper limit on the 498 keV E0 branch.

5. Summary and conclusions

The β decay of ^{100}Y was studied using the GRIFFIN spectrometer at TRIUMF-ISAC. Analysis of γ–γ angular correlations led to firm spin assign-

ments and the extraction of E2/M1 mixing ratios. Relative B(E2) values for the decay of the 2_2^+ and 2_3^+ states were determined. Literature lifetimes for the 2_1^+ and 0_2^+ states were used as input to a two-state-mixing calculation, and it was found that the decay pattern of the 2_2^+ state could not be reproduced. A limit on the $0_3^+ \to 0_2^+$ E0 intensity was also determined.

This work was supported in part by the Natural Sciences and Engineering Research Council of Canada. The GRIFFIN infrastructure has been funded jointly by the Canada Foundation for Innovation, the British Columbia Knowledge Development Fund (BCKDF), the Ontario Ministry of Research and Innovation (ON-MRI), TRIUMF, and the University of Guelph. TRIUMF receives federal funding via a contribution agreement through the National Research Council Canada (NRC). This research was also partially supported by the U.S. Department of Energy, Office of Science, Office of Nuclear Physics, under contract number DE-AC02-06CH11357 and by the U.S. National Science Foundation under grant No. PHY-2209178.

REFERENCES

[1] P. Campbell *et al.*, *Phys. Rev. Lett.* **89**, 082501 (2002).
[2] P.E. Garrett, M. Zielińska, E. Clément, *Prog. Part. Nucl. Phys.* **124**, 103931 (2022).
[3] T. Togashi, Y. Tsunoda, T. Otsuka, N. Shimizu, *Phys. Rev. Lett.* **117**, 172502 (2016).
[4] N. Gavrielov, A. Leviatan, F. Iachello, *Phys. Rev. C* **105**, 014305 (2022).
[5] E. Clément *et al.*, *Phys. Rev. Lett.* **116**, 022701 (2016).
[6] W. Urban *et al.*, *Phys. Rev. C* **99**, 064325 (2019).
[7] W. Urban *et al.*, *Phys. Rev. C* **100**, 014319 (2019).
[8] J. Wu *et al.*, *Phys. Rev. C* **109**, 024314 (2024).
[9] B. Singh, J. Chen, *Nucl. Data Sheets* **172**, 1 (2021).
[10] A.B. Garnsworthy *et al.*, *Nucl. Instrum. Methods Phys. Res. A* **918**, 9 (2019).
[11] D. Kalaydjieva, Ph.D. Thesis, Université Paris-Saclay, 2023.
[12] J.K. Smith *et al.*, *Nucl. Instrum. Methods Phys. Res. A* **922**, 47 (2019).
[13] S. Robinson, *Nucl. Instrum. Methods Phys. Res. A* **292**, 386 (1990).
[14] F.K. Wohn *et al.*, *Phys. Rev. C* **33**, 677 (1986).
[15] T. Kibédi, A.B. Garnsworthy, J.L. Wood, *Prog. Part. Nucl. Phys.* **123**, 103930 (2022).
[16] E. Clément *et al.*, *Phys. Rev. C* **75**, 054313 (2007).